JOC Article
pubs.acs.org/joc

Effective Enlargement of Fluorescence Resonance Energy Transfer of Poly-Porphyrin Mediated by β-Cyclodextrin Dimers

Zhuo-Yi Gu, Dong-Sheng Guo, Mo Sun, and Yu Liu*

Department of Chemistry, State Key Laboratory of Elemento-Organic Chemistry, Nankai University, Tianjin, 300071, People's Republic of China

yuliu@nankai.edu.cn

Received March 1, 2010

Downloaded via NANKAI UNIV on November 17, 2018 at 08:39:26 (UTC).
See https://pubs.acs.org/sharingguidelines for options on how to legitimately share published articles.

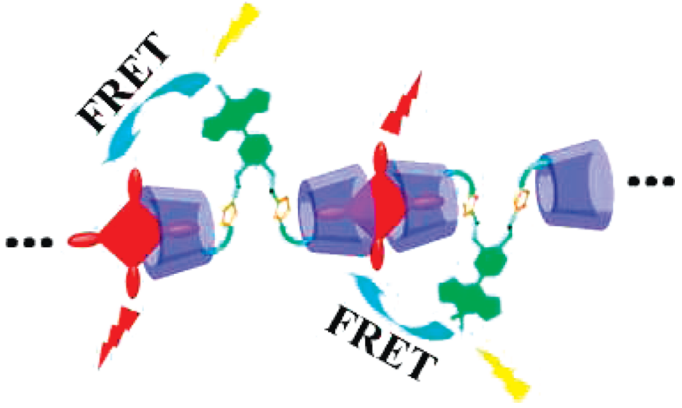

4,4-Difluoro-4-bora-3a,4a-diaza-*s*-indacene bridged bis(permethyl-β-cyclodextrins) **1** was synthesized successfully through click chemistry, and it forms a well-defined linear assembly with 5,10,15,20-tetrakis(4-sulfonatophenyl)porphyrin **2** via extremely strong host−guest interactions, which was identified by the methods of UV−vis, NMR, AFM, and TEM, respectively. Furthermore, the fluorescence resonance energy transfer from host spacer to porphyrin guest was investigated, showing that the energy transfer quantum yield is high to 94% in virtue of such a noncovalent path.

Introduction

Fluorescence resonance energy transfer (FRET) is a significant process not only in nature but also for building artificial devices.[1] In photosynthesis, FRET acts as the former key step before electron transfer, where the light-harvesting molecules absorb light energy of appropriate wavelength and transport to the reaction center.[2] In parallel, FRET is also ubiquitous in many artificial optical, electronic, and optoelectronic systems, including photoelectric conversion in solar energy cells, information accessing with a variety of molecular apparatus, and detection of analytes with molecular-based sensors.[3] Three essential factors must be satisfied to fulfill effective FRET: (a) donor and acceptor molecules must be in close proximity (1−10 nm); (b) the absorption spectrum of the acceptor overlaps the fluorescence emission spectrum of the donor as much as possible; and (c) donor and acceptor transition dipole orientations are approximately parallel.[4] Most of these energy-transfer dyads are built by covalent conjugations, which exhibit advantages of accurately controlling both the location and orientation

(1) (a) Wagner, R. W.; Lindsey, J. S. *J. Am. Chem. Soc.* **1994**, *116*, 9759–9760. (b) Hahn, U.; Gorka, M.; Vögtle, F.; Vicinelli, V.; Ceroni, P.; Maestri, M.; Balzani, V. *Angew. Chem., Int. Ed.* **2002**, *41*, 3595–3598. (c) Bandichhor, R.; Petrescu, A. D.; Vespa, A.; Kier, A. B.; Schroeder, F.; Burgess, K. *J. Am. Chem. Soc.* **2006**, *128*, 10688–10689. (d) Hippius, C.; Schlosser, F.; Vysotsky, M. O.; Böhmer, V.; Wüthner, F. *J. Am. Chem. Soc.* **2006**, *128*, 3870–3871. (e) Zhang, X.-L.; Xiao, Y.; Qian, X.-H. *Angew. Chem., Int. Ed.* **2008**, *47*, 8025–8029.

(2) D'Souza, F.; Smith, P. M.; Zandler, M. E.; McCarty, A. L.; Itou, M.; Araki, Y.; Ito, O. *J. Am. Chem. Soc.* **2004**, *126*, 7898–7907.

(3) (a) Holten, D.; Bocian, D. F.; Lindsey, J. S. *Acc. Chem. Res.* **2002**, *35*, 57–69. (b) Saha, S.; Stoddart, J. F. *Chem. Soc. Rev.* **2007**, *36*, 77–92. (c) Wasielewski, M. R. *J. Org. Chem.* **2006**, *71*, 5051–5066. (d) Fukuzumi, S. *Phys. Chem. Chem. Phys.* **2008**, *10*, 2283–2297. (e) Kikuchi, K.; Takakusa, H.; Nagano, T. *Trends Anal. Chem.* **2004**, *23*, 407–415. (f) Liu, J.-Y.; Yeung, H.-S.; Xu, W.; Li, X.; Ng, D. K. P. *Org. Lett.* **2008**, *10*, 5421–5424.

(4) (a) Zahavy, E.; Fisher, M.; Bromberg, A.; Olshevsky, U. *Appl. Environ. Microbiol.* **2003**, *69*, 2330–2339. (b) Fabricio, A.-L.; Cosultchi, A.; Pérez, E. *Energy Fuels* **2005**, *19*, 477–484.

Published on Web 05/05/2010 DOI: 10.1021/jo100351f

© 2010 American Chemical Society

of chromophores.[5] Alternatively, the noncovalent assembly, regarded as the rather simple approach to organize donor/acceptor chromophores together, has gained much less attention, possibly because it remains somewhat difficult to introduce an energetic gradient in self-assembled species.[6] Weiss and co-workers designed a linear porphyrin architecture, where N-unsubstituted imidazole coordinated to zinc porphyrin besides hydrogen bonds between phenanthroline and imidazole make the donor and acceptor close, which leads to energy transfer from zinc porphyrin to free base porphyrin.[6] Li and co-workers constructed a series of water-soluble dendrimers, where FRET from anthracene to peripheryl naphthyl chromophore occurred through hydrophobic interactions.[7]

Cyclodextrins (CDs), a class of cyclic oligosaccharides with 6−8 D-glucose units linked by α-1,4-glucose bonds, are extensively used as not only excellent receptors for molecular recognition but also sophisticated building blocks for spectacular supramolecular architectures.[8] In the past decade, CDs also have been employed in building noncovalent FRET systems.[9] Lehn and co-workers reported the FRET by β-CD bearing seven naphthoyl chromophores complexing with merocyanine dye, showing perfect 100% efficiency with a *n*:1 (donor/acceptor) model.[9a] Kano and co-workers reported free-base porphyrin bridged four permethylated β-CDs and explored their energy transfer behaviors through a small inclusion compound by complexing with Zn-porphyrin, where different donors to one acceptor may be responsible for the discrepancy of transfer efficiency.[9b] Ng and co-workers investigated the complexation between phthalocyanin bridged two permethylated β-CDs and tetrasulfonated porphyrin, where a head-to-tail polymeric assembly was logically inferred, exhibiting singlet−singlet energy transfer besides electron transfer.[9c] Although with these investigations there is no specific report on the FRET in the CD-based assembly with multiple well-organized donors and acceptors, the comparison of energy transfer between assembly and 1:1 complex is still unexplored.

Herein, we fabricated a well-ordered linear assembly from 4,4-difluoro-4-bora-3a,4a-diaza-*s*-indacene (BODIPY) bridged bis(permethyl-β-cyclodextins) **1** and 5,10,15,20-tetrakis(4-sulfonatophenyl)porphyrin **2**, exhibiting highly efficient FRET from BODIPY donor to porphyrin acceptor. BODIPY was employed as an energy donor because it has strong UV absorption that emits a relatively sharp fluorescence peak with high quantum yield, and is relatively insensitive to the polarity and pH, and reasonably stable to physiological conditions.[10] Porphyrin was used as the energy acceptor because its Q-band absorption overlaps BODIPY's emission. Moreover, porphyrins are famous photosynthetic molecules used not only as the antenna but also as the photosynthetic center.[11] Although the present system is built by noncovalent approach, its accuracy of controlling location and orientation can compare well with that by the covalent approach because of the exceptionally strong binding ability, unambiguous binding stoichiometry, and geometry of permethyl-β-cyclodextin (PMCD) with **2**.[12] In addition, the obtained assembly has benign water-solubility, allowing its potential application in biological system.

SCHEME 1. The Synthetic Routes of 1 and 3 and Structural Illustration of 2 and 3

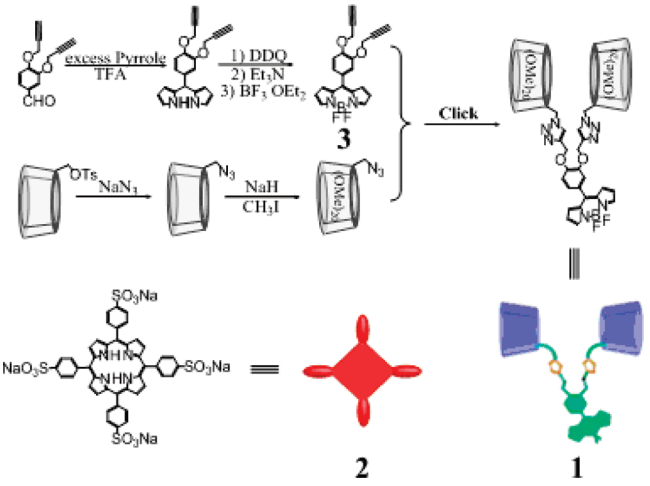

Result and Discussion

Synthesis of BODIPY-Bridged Bis(permethyl-β-cyclodextins) 1. The BODIPY segment was synthesized through the analogical method reported in the literature.[13] 3,4-Di-(prop-2-ynyloxy)benzaldehyde reacted with excess pyrrole with TFA as an acid catalyst, further oxidated by DDQ, and reacted with $BF_3 \cdot OEt_2$ to produce the desired compound **3**. Compound **1** was synthesized by 6-deoxy-6-azide-permethyl-β-cyclodextrin reacting with **3**, using an improved version of Huisgen cycloaddition named "click" reaction catalyzed by CuI in DMF with a satisfactory yield (Scheme 1), and characterized by ^{1}H NMR, ^{13}C NMR, 2D NOESY, MALDI-HRMS, and elemental analysis. PMCD was employed because of its high binding ability to water-soluble porphyrins in aqueous solution, which is regarded as the key point to construct supramolecular architectures.

Construction of Supramolecular Assembly from 1 and 2. UV−vis, NMR, AFM, and TEM measurements were

(5) (a) Shiragami, T.; Tanaka, K.; Andou, Y.; Tsunamia, S.; Matsumoto, J.; Luo, H.-X.; Araki, Y.; Ito, O.; Inoue, H.; Yasuda, M. *J. Photochem. Photobiol., A* **2005**, *170*, 287–297. (b) Lammi, R. K.; Wagner, R. W.; Ambroise, A.; Diers, J. R.; Bocian, D. F.; Holten, D.; Lindsey, J. S. *J. Phys. Chem. B* **2001**, *105*, 5341–5352.

(6) Koepf, M.; Trabolsi, A.; Elhabiri, M.; Wytko, J. A.; Paul, D.; Albrecht-Gary, A. M.; Weiss, J. *Org. Lett.* **2005**, *7*, 1279–1282.

(7) Zeng, Y.; Li, Y.; Li, M.; Yang, G.; Li, Y. *J. Am. Chem. Soc.* **2009**, *131*, 9100–9106.

(8) (a) Harada, A. *Acc. Chem. Res.* **2001**, *34*, 456–464. (b) Douhal, A. *Chem. Rev.* **2004**, *104*, 1955–1976. (c) Wenz, G.; Han, B.-H.; Müller, A. *Chem. Rev.* **2006**, *106*, 782–817. (d) Liu, Y.; Chen, Y. *Acc. Chem. Res.* **2006**, *39*, 681–691.

(9) (a) Jullien, L.; Canceill, J.; Valeur, B.; Bardez, E.; Lefèvre, J.-P.; Lehn, J.-M.; Marchi−Artzner, V.; Pansu, R. *J. Am. Chem. Soc.* **1996**, *118*, 5432–5442. (b) Kano, K.; Nishiyabu, R.; Yamazaki, T.; Yamazaki, I. *J. Am. Chem. Soc.* **2003**, *125*, 10625–10634. (c) Leng, X.; Choi, C.-F.; Lo, P.-C.; Ng, D. K. P. *Org. Lett.* **2007**, *9*, 231–234.

(10) (a) Loudet, A.; Burgess, K. *Chem. Rev.* **2007**, *107*, 4891–4932. (b) Ulrich, G.; Ziessel, R.; Harriman, A. *Angew. Chem., Int. Ed.* **2008**, *47*, 1184–1201.

(11) (a) Ward, M. D. *Chem. Soc. Rev.* **1997**, *26*, 365–375. (b) Choi, M.-S.; Yamazaki, T.; Yamazaki, I.; Aida, T. *Angew. Chem., Int. Ed.* **2004**, *43*, 150–158. (c) Boyd, P. D. W.; Reed, C. A. *Acc. Chem. Res.* **2005**, *38*, 235–242.

(12) (a) Kano, K.; Nishiyabu, R.; Asada, T.; Kuroda, Y. *J. Am. Chem. Soc.* **2002**, *124*, 9937–9944. (b) Deng, W.; Onji, T.; Yamaguchi, H.; Ikeda, N.; Harada, A. *Chem. Commun.* **2006**, 4212–4214.

(13) Baruah, M.; Qin, W. W.; Basarić, N.; De Borggraeve, W. M.; Boens, N. *J. Org. Chem.* **2005**, *70*, 4152–4157.

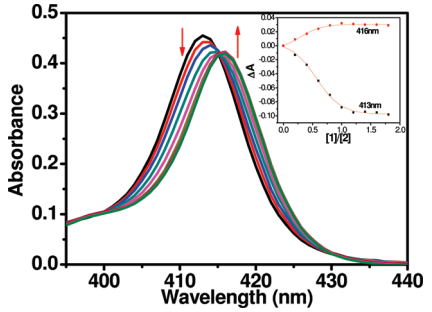

FIGURE 1. Soret band spectral changes of **2** (1.0×10^{-6} M) upon addition of **1** (0−2 equiv) in pH 7.2 phosphate buffer solution at 25 °C.

performed respectively to confirm the host−guest interactions between **1** and **2**, binding stoichiometry, binding geometry, and the intuitionistic morphology. The titration of UV−vis spectroscopy (Figure 1) shows that the Soret band absorption of **2** changes gradually by continuous addition of **1**. The absorptivity at 413 nm decreases and a new absorption band appears at 416 nm, resulting in an isosbestic point appearing at 415 nm. The appreciable bathochromic shift of the Soret band reflects the electronic perturbations arising from solvent effects and from changes in the solvent−solute dipole interactions caused by reduced exposure of the solute to water when **2** was included into the cavity of **1**.[14] Moreover, the absorbance changes of **2** almost reach the maximum upon addition of 1 equiv of **1**, which indicate the formation of a stable 1:1 complex between **1** and **2**, simultaneously taking the concentrations of host and guest into account. The host−guest binding stoichiometry was further identified by the Job's plot (see the Supporting Information, Figure S7), where the maximum value of ΔA (complex-induced changes of absorbance) appears at a porphyrin molar fraction of 0.5. This is in accordance with previous results that two PMCD units can concurrently include one porphyrin backbone.[15]

The structures of host **1** and complex **1**·**2** were examined by ^{1}H NMR and 2D NOESY, respectively. Judged from the NOESY spectra of free **1** (Figure 2a,b), the BODIPY spacer is self-included into the cavity of PMCD as clear cross-peaks between protons of BODIPY and protons of PMCD were observed. Moreover, there is strong correlation between H_a and H_b, while not between H_a and H_c (Figure 2c). Combining this phenomenon and steric hindrance effect, PMCD of the meta-position is more reasonable than that of the para-position to include the BODIPY unit. The structural modulation of **1** according to the energy minimum method also reveals that the hindrance in space embarrasses the *p*-PMCD to complex with the BODIPY spacer. The self-included structure of **1** is illustrated in Figure 2d.

Complexing with porphyrin **2**, some protons of PMCD show pronounced upfield shift arising from the ring current effect of the aromatic nuclei of porphyrin (see the Supporting Information, Figure S8). More detailed information from the 2D NOESY spectrum (Figure 3) shows that the protons of δ 8.7−8.9 ppm, assigned to the pyrrole protons, exhibit

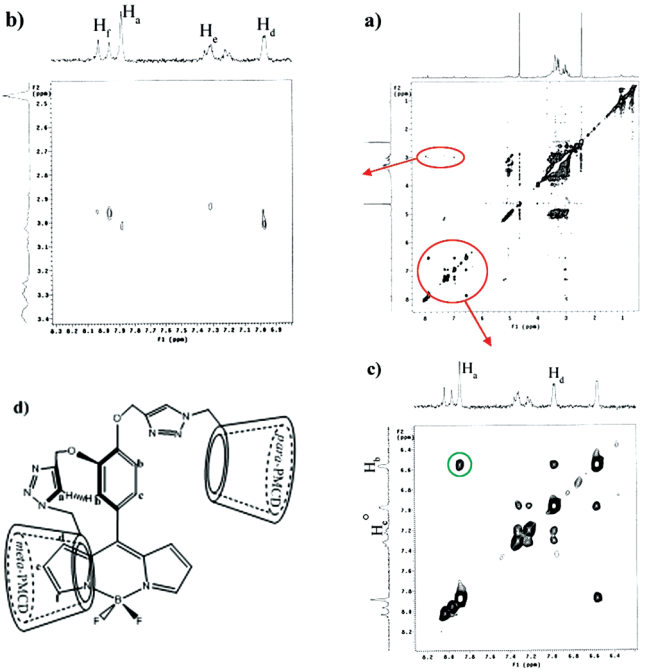

FIGURE 2. 2D NOESY spectra of **1** in 10% DMSO-d_6−D_2O at 25 °C with a mixing time of 220 ms. Panels b and c are enlarged areas of panel a. (d) Deduced structure of **1**.

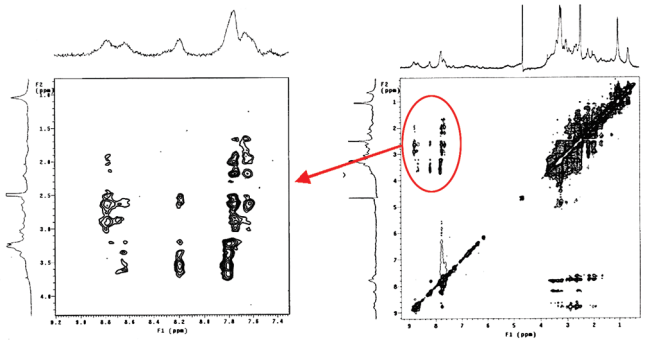

FIGURE 3. 2D NOESY spectra of **1**·**2** in 10% DMSO-d_6−D_2O at 25 °C with a mixing time of 220 ms.

multiple cross peaks with the PMCD protons of the secondary OCH_3, indicating that **2** is deeply included into the cavities of **1** from the wide opening. Meanwhile, the self-included cross peaks between BODIPY and PMCD disappear, and therefore, BODIPY is compelled out of the cavity of PMCD as a result of the strong inclusion ability of PMCD with porphyrins.

Three possible complexation modes can be assumed for the present host−guest system, that is, 1:1 simple complex, 2:2 molecular wedge,[16] and *n*:*n* 1D wirelike aggregation. The first one can be reasonably excluded in view of the steric hindrance, as it has been proved by NMR results that porphyrin penetrates into the PMCD cavity from the wide edge.[15] We performed the AFM and TEM measurements to identify which one is more acceptable among the last two possible modes according to the complex morphology.

(14) Lang, K.; Mosinger, J.; Wagnerová, D. M. *Coord. Chem. Rev.* **2004**, *248*, 321–350.
(15) Liu, Y.; Ke, C.-F.; Zhang, H.-Y.; Cui, J.; Ding, F. *J. Am. Chem. Soc.* **2008**, *130*, 600–605.
(16) Sasaki, K.; Nakagawa, H.; Zhang, X.-Y.; Sakurai, S.; Kano, K.; Kuroda, Y. *Chem. Commun.* **2004**, 408–409.

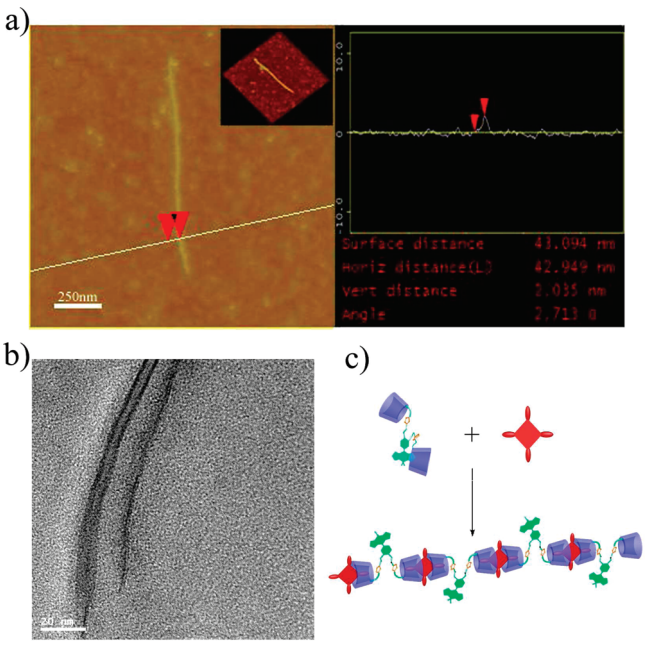

FIGURE 4. (a) AFM image of assembly **1**·**2**; (b) TEM images of assembly **1**·**2**; and (c) diagrammatic representation of the process that forms 1D wirelike aggregation.

Figure 4a shows that a 1D linear morphology was observed when mixing **1** and **2** at an equivalent molar ratio. The height is about 2.0 nm, which corresponds to the size of both BODIPY bridged PMCDs **1** and porphyrin **2**. The width appears larger than its real size due to the broadening effect produced by the AFM tip.[17] Similar linear morphology was also found in TEM images (Figure 4b, as well as Figure S9 in the Supporting Information). Consequently, combining the results of UV−vis, NMR, and microscopy together, we reasonably infer that the complexation of **1** and **2** leads to *n*:*n* 1D wirelike aggregation as illustrated in Figure 4c.

Fluorescence Resonance Energy Transfer from BODIPY to Porphyrin in Assembly 1·2. Figure 5 shows the steady-state fluorescence emission spectrum of **1** and the Q-band absorption spectrum of **2**. All the Q-band absorptions fall into the emission band of BODIPY. It is, therefore, expected that assembly **1**·**2** should exhibit an efficient through-space energy transfer. The general covalent approach, especially via unsaturated bond, may make the donor and acceptor parts become electronically conjugated to form new, extended chromophores.[18] The noncovalent approach employed here can avoid such conjugation. Moreover, porphyrin is protected by the inclusion of PMCD, which can therefore depress the unfavorable factors for FRET, such as $\pi\cdots\pi$ stacking among chromophores and formation of charge transfer complexes.

The energy transfer process in assembly **1**·**2** was examined by steady-state fluorescence spectroscopy. Figure 6 shows the emission spectra of **1** in the absence and presence of **2** with different molar ratios. The excitation wavelength was chosen as 470 nm to avoid the Q-band absorption of **2**. Along with

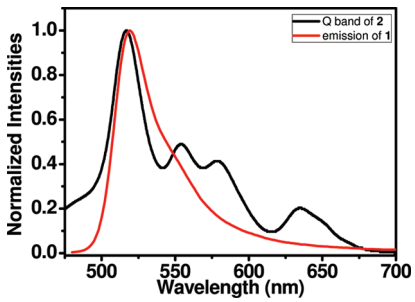

FIGURE 5. Normalized spectra of Q-band absorption of **2** and emission of **1** in pH 7.2 phosphate buffer solution at 25 °C.

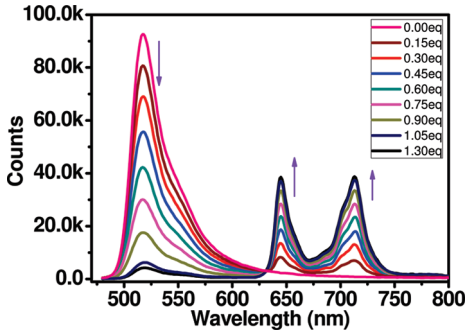

FIGURE 6. Fluorescence spectral changes of **1** (1×10^{-6} M) upon addition of **2** in pH 7.2 phosphate buffer solution at 25 °C, λ_{ex} = 470 nm.

the augmentation of **2**, the emission of **1** peaked at 520 nm decreases gradually while the emission of **2** increases in proportion. Both the decreasing and increasing changes level off upon addition of 1 equiv of **2**. The green fluorescence of BODIPY is almost quenched while only the red fluorescence of **2** is presented (Scheme 2). However, no appreciable emission of porphyrin was observed when free **2** was excited at 470 nm. The inclusion complex of **2** with PMCD also presents the corresponding red fluorescence upon excitation at 470 nm, but the emission intensity is 7 times weaker than that of assembly **1**·**2** at the same concentration (see the Supporting Information, Figure S10b). These results demonstrated undoubtedly that the FRET process existed in **1**·**2**. We further performed the fluorescence spectra of the precursor BODIPY **3** in the absence and presence of **2** (see the Supporting Information, Figure S10a) in order to examine the effect of diffusional collision, showing that the emission of **3** is almost unchanged upon addition of 1 equiv of **2**. It can be seen that the cavity of PMCD plays a predominant role in the energy-transfer process that draws the donor and acceptor chromophores together. The noncovalent energy transfer is a tandem process that follows the inclusion complexation.

Further, the excitation spectra of **1**·**2** and **2** were examined by monitoring the emission at 713 nm (Figure 7). A typical excitation spectrum of **2** was observed, which is similar in shape to the absorption spectrum of **2**. The excitation spectrum of **1**·**2**, similar to the corresponding absorption spectrum too, showed obvious hypochromatic shift centered at 509 nm as compared with the Q-band in **2** (centered at 516 nm). More importantly, the new excitation signals ranging from 450 to 500 nm relative to **2** were similar to the absorption spectrum of **1**. It is also noted that the absorption coefficient of **1** is much larger than that of **2** in

(17) (a) Kirby, A. R.; Gunning, A. P.; Morris, V. J. *Biopolymers* **1996**, *38*, 355–366. (b) Rivetti, C.; Codeluppi, S. *Ultramicroscopy* **2001**, *87*, 55–66.

(18) Jiao, G.-S.; Thoresen, L. H.; Kim, T. G.; Haaland, W. C.; Gao, F.; Topp, M. R.; Hochstrasser, R. M.; Metzker, M. L.; Burgess, K. *Chem.—Eur. J.* **2006**, *12*, 7816–7826.

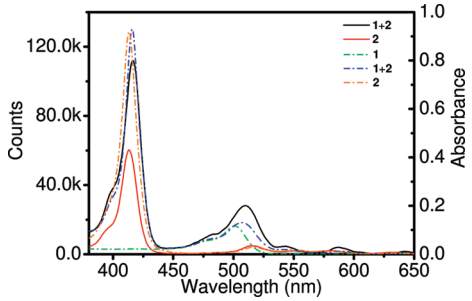

FIGURE 7. Excitation spectra of **1**·**2** and **2** (solid line) by monitoring the emission wavelength at 713 nm and absorption spectra of **1**, **2**, and **1**·**2** (dashed line) in pH 7.2 phosphate buffer solution at 25 °C; the concentration of **2** was 1×10^{-6} M in excitation spectra and 5×10^{-6} M in absorption spectra, respectively.

SCHEME 2. Diagrammatic representation of the energy-transfer processes in assembly 1·2 and complex 1·2·PMCD

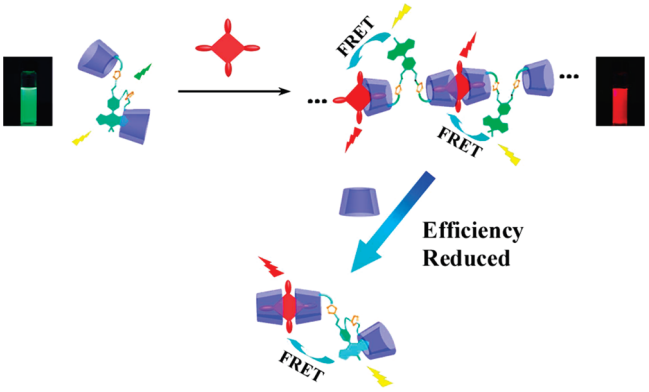

the region of 450−550 nm, in other words, the absorption spectrum of **1**·**2** originates mainly from the contribution of **1**. As a result, the porphyrin's fluorescence emission in **1**·**2** should arise mainly from the excited species of **1**. We also performed the excitation spectrum of **2** in the presence of 2 equiv of PMCD. Although its signal is more intensive than that of free **2**, the **2**·$(PMCD)_2$ can hardly be excited with wavelengths shorter than 500 nm. These results of excitation spectra further proved the process of energy transfer in **1**·**2** that the excitation of BODIPY at 470 nm leads to the emission of porphyrin directly.

The efficiency of energy transfer E can be defined as the fraction of donor molecules de-excited via energy transfer to the acceptor, which equals[19]

$$E = \left(1 - \frac{I_{DA}}{I_D}\right) = \left(1 - \frac{\tau_{DA}}{\tau_D}\right) = \left(1 - \frac{\Phi_{DA}}{\Phi_D}\right) \qquad (1)$$

where I_{DA}, τ_{DA}, and Φ_{DA} are the intensity of fluorescence, lifetime, and quantum yield, respectively, of the donor in the presence of acceptor, and I_D, τ_D, and Φ_D in the absence of acceptor. The I_D and I_{DA} value were measured as 92618 counts and 6389 counts, respectively (Figure 6). The absolute fluorescence quantum yield (Φ_F) of BODIPY decreases seriously from 0.155 in **1** to 0.009 in **1**·**2**, accounting for

(19) (a) Jensen, K. K.; van Berlekom, S. B.; Kajanus, J.; Martensson, J.; Albinsson, B. *J. Phys. Chem. A* **1997**, *101*, 2218–2220. (b) Kilsa, K.; Kajanus, J.; Martensson, J.; Albinsson, B. *J. Phys. Chem. B* **1999**, *103*, 7329–7339.

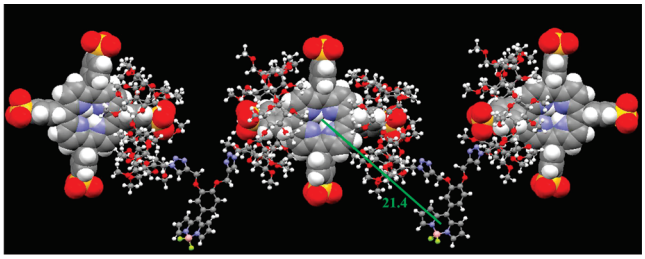

FIGURE 8. Possible structure through molecular modulation of **1**·**2** and the measured center distance between **2** and BODIPY.

the high efficiency of energy transfer (see the Supporting Information, Figure S11). According to eq 1, the value of E was calculated as 93% or 94% by using the measured I or Φ method.

The transfer efficiency of FRET is known as distance-dependent, which was widely used not only in biochemistry but also in material science.[20] The donor-to-acceptor energy transfer mainly depends on three parameters: distance, orientation factor, and overlap integral of donors' emission and acceptors' absorption.[21] Förster argued the transfer efficiency E as follows:

$$E = \frac{nR_0^6}{nR_0^6 + r_{DA}^6} = \frac{1}{1 + (r_{DA}^6/nR_0^6)} \qquad (2)$$

where R_0 is the Förster distance at which the energy transfer is at 50%, r_{DA} is the donor-to-acceptor distance, and n is the molar ratio of acceptors to donors. Also, R_0 can be calculated as the following equations:

$$R_0 = (8.79 \times 10^{-5})[k^2 \eta^{-4} \Phi_D J(\lambda)]^{1/6} \qquad (3)$$

$$J(\lambda) = \frac{\int \varepsilon_A(\lambda) f_D(\lambda) \lambda^4 \, d\lambda}{\int f_D(\lambda) \, d\lambda} \qquad (4)$$

where k^2 is the orientation factor related to the relative angle between donor and acceptor transition dipoles, taken to be $^2/_3$, η is the refractive index of the medium, taken to be 1.4 in aqueous media,[22] and $J(\lambda)$ is the normalized spectral overlap of the donor emission (f_D) and the acceptor absorption (ε_A).

In **1**·**2**, the spectral overlap integral $J(\lambda)$ was calculated to be 4.88×10^{-14} $M^{-1} \cdot cm^3$, and therefore the R_0 value was estimate to be 32.9 Å. Together with the energy transfer efficiency $E = 0.94$, we can easily calculate the center distance between the donor and acceptor as about 20.8 Å, which is similar to the optimized molecular modulation result from the minimized energy method (21.4 Å, Figure 8).

Further, the kinetic parameters within the energy transfer process can be expressed as:

$$E = \frac{k_T}{k_T + k_d} = \frac{1}{1 + (k_d/k_T)} = \frac{1}{1 + (1/\tau_D k_T)} \qquad (5)$$

(20) (a) Medintz, I. L.; Clapp, A. R.; Mattoussi, H.; Goldman, E. R.; Fisher, B.; Mauro, J. M. *Nat. Mater.* **2003**, *2*, 630–638. (b) Medintz, I. L.; Uyeda, H. T.; Goldman, E. R.; Mattoussi, H. *Nat. Mater.* **2005**, *4*, 435–446. (c) Scheller, F. W.; Wollenberger, U.; Warsinke, A.; Lisdat, F. *Curr. Opin. Biotechnol.* **2001**, *12*, 35–40.

(21) Zhang, X.; Rehm, S.; Safont-Sempere, M. M.; Würthner, F. *Nat. Chem.* **2009**, *1*, 623–629.

(22) McLaurin, E. J.; Greytak, A. B.; Bawendi, M. G.; Nocera, D. G. *J. Am. Chem. Soc.* **2009**, *131*, 12994–13001.

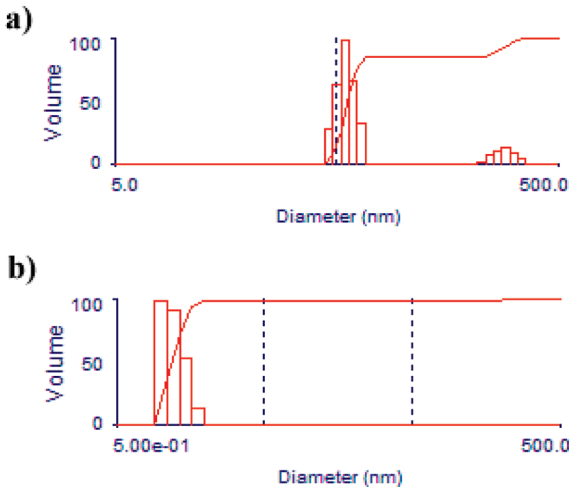

FIGURE 9. Diameter distributions of **1**·**2** (a) before and (b) after adding 1 equiv of PMCD in aqueous solution at 25 °C.

where k_T is the energy-transfer rate of the FRET process, τ_D is the lifetime of the donor in the absence of acceptor, and k_d is the inverse lifetime in the absence of acceptor. Note that combining eqs 2 and 5 yields:

$$k_T = \tau_D^{-1} \frac{nR_0^6}{r_{DA}^6} \quad (6)$$

Free **1** gives two lifetimes, 1.62 and 7.75 ns, representing BODIPY out of and in the cavity of PMCD, respectively (see the Supporting Information, Figure S12), and therefore, according to eq 6, k_T was calculated to be 9.67×10^9 s^{-1}, where the lifetime of 1.62 ns was engaged as BODIPY spacer is compelled out of the cavity of host by porphyrin guest in assembly **1**·**2**.

Assembly 1·2 Disassembled into Ternary 1·2·PMCD by Adding PMCD. To further investigate the advantage of the assembly in energy-transfer efficiency, 1 equiv of PMCD was added to the **1**·**2** system, potentially leading to the 1:1:1 **1**·**2**·PMCD complex (Scheme 2) as K_S(PMCD·**2**) ($> 10^8$ M^{-1}) is too large to be measured.[12a] The negative ion mode ESI mass spectra of **1**·**2** before and after adding 1 equiv of PMCD (see the Supporting Information, Figure S14) prove the formation of **1**·**2**·PMCD complex. A peak at 1404.06 was found when 1 equiv of PMCD was added to **1**·**2**, which stands for $[\mathbf{1}+\mathbf{2}+\text{PMCD}-4\text{Na}^+]^{4-}$. No peak assigned to the **2**·$(PMCD)_2$ complex was observed. There is still the peak at 1046.88 ($[\mathbf{1}+\mathbf{2}-4\text{Na}^+]^{4-}$), indicating that the addition of PMCD does not disassemble the linear aggregation to the 1:1:1 complex thoroughly or may result in oligomer-like aggregations.[23] However, the residual **1**·**2** aggregation exists just as a minor product with almost negligible quantity. The dynamic light scattering (DLS) experiment of **1**·**2** (Figure 9a) shows that two main groups of different diameters were observed, one is in the range of 46−64 nm, the other in the range of 224−339 nm, proving the formation of large-scaled assembly in solution. Upon addition of 1 equiv of PMCD into **1**·**2**, one can only observe the particles with diameters from 1 to 2 nm which may correspond to the **1**·**2**·PMCD complex, and also possibly, the noise of the backgroup.

(23) Ma, X.; Tian, H. *Chem. Soc. Rev.* **2010**, *39*, 70–80.

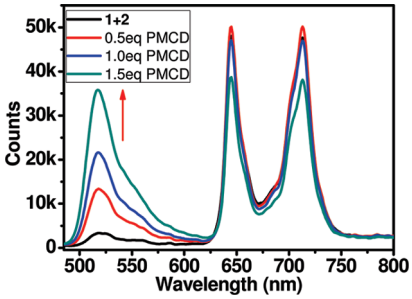

FIGURE 10. Fluorescence spectral changes of **1**·**2** (1×10^{-6} M) upon addition of PMCD in pH 7.2 buffer solution at 25 °C, λ_{ex} = 470 nm.

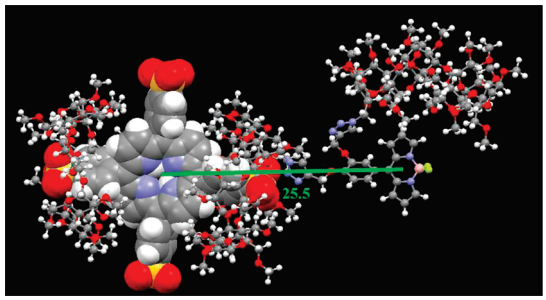

FIGURE 11. Possible structure through molecular modulation of **1**·**2**·PMCD and the measured center distance between **2** and BODIPY.

In any case, no signal of huge assembly was observed upon addition of PMCD (Figure 9b).

Fluorescence Resonance Energy Transfer from BODIPY to Porphyrin in Ternary 1·2·PMCD. When gradually adding PMCD into the solution of **1**·**2**, the fluorescence of BODIPY recovered to some extent (Figure 10). Two factors can be assumed for this: one is that the inclusion of PMCD enhanced the emission intensity of BODIPY; the other is that the addition of PMCD destroyed partially the assembly, and then depressed the efficiency of energy transfer. The following controlling experiments excluded the former possibility. Only a little ruleless change was observed even though excess PMCD was added to the solution of **1** (see the Supporting Information, Figure S15). On the other hand, the emission of **2** changes a little until 1.0 equiv of PMCD was added, whereas it decreases suddenly (25% percent) when 1.5 equiv of PMCD was added (Figure 10). The sharp quenching of **2** with over 1.0 equiv of PMCD is acceptable in that the excess addition of PMCD would lead to the formation of 1:2 complex **2**·$(PMCD)_2$, and then energy transfer becomes less effective because some porphyrin deviating from assembly of **1**·**2** can no longer receive the energy of BODIPY. According to the aforementioned ESI-MS and DLS results, assembly **1**·**2** turns to ternary complex **1**·**2**·PMCD mostly when 1 equiv of PMCD was added. Comparing the fluorescence of BODIPY and quantum yield of **1** (0.026, see the Supporting Information, Figure S13) between **1**·**2**·PMCD and **1**·**2**, it can be found that the energy transfer quantum yield in **1**·**2**·PMCD is not as high as that in **1**·**2**, which is only 83% as compared with that in **1**·**2** (94%), and the center distance between the donor and acceptor in the ternary system was calculated to be 25.2 Å. This is a reasonable

result that in the assembly, the two PMCDs of **1** should adopt a special orientation in order to maintain the assembly wirelike shape while there is no such conformational limitation in the ternary system, where PMCD of **1** can rotate freely and thus the donor and acceptor in **1·2·**PMCD would become further away than in **1·2**. A possible optimized molecule modulation of **1·2·**PMCD was presented in Figure 11 and the distance was estimated to be 25.5 Å, which is similar to the calculated result. Further, the energy transfer rate in **1·2·**PMCD was also calculated as 3.06×10^9 s^{-1}, which decreased sharply compared with that of **1·2** (9.67×10^9 s^{-1}). These results mentioned above convincingly illustrate the donor/acceptor in linear assembly would adopt the "proximate" form and therefore have much higher energy transfer efficiency and rate than that in the ternary system, which may adopt the "distal" form. Consequently, one can reasonably infer that the assembly system with multiple donors and acceptors shows more advantage to enhance the energy transfer efficiency than the simple system with a single donor and acceptor.

Conclusion

In summary, a supramolecular wirelike assembly was constructed by BODIPY bridged PMCDs **1** upon complexation with porphyrin guest **2**, where multiple energy-transfer donors and acceptors are regularly arrayed. The tandem energy transfer occurs in the assembly with a high efficiency of 94%. Several factors contribute synergistically to the high FRET efficiency: (a) the perfect matching of spectra between BODIPY donor and porphyrin acceptor; (b) the suitable spatial array of donor and acceptor mediated by cyclodextrin; (c) the inclusion of cyclodextrin protects the D/A chromophores from $\pi\cdots\pi$ stacking and charge-transfer complexation; and (d) more interestingly, the well-designed wirelike model shows more favorability for energy transfer than the simple 1:1 model. Consequently, the present results not only pave a noncovalent way to build highly ordered and stable nanoarchitectures with multiple donors and acceptors, but also provide an improved asembly model for constructing highly effective light-harvesting systems.

Experimental Section

Materials. β-Cyclodextrin was purchased and recrystallized from water twice and then dried under vacuum at 85 °C for 24 h before use. 5,10,15,20-Tetrakis(4-sulfonatophenyl)porphyrin (**2**) was commercially available with high purity (>99%) and used as received. Pyrrole was commercially available and freshly distilled before use. Other materials and solvents were commercially available. Column chromatography was performed on silica gel (200−300 mesh). The phosphate buffer solution of pH 7.2 was prepared by dissolving disodium hydrogen phosphate ($Na_2HPO_4 \cdot 12H_2O$, 51.57 g) and sodium dihydrogen phosphate ($NaH_2PO_4 \cdot 2H_2O$, 8.73 g) in distilled deionized water (2 L) to make a 0.1 M solution. The pH value of the buffer solution was verified on a pH-meter calibrated with two standard buffer solutions.

Measurements. NMR spectra were performed on a 300 M spectrometer. Mass spectra were performed on either an IonSpec QFT-MALDI MS or an IonSpec QFT-ESI MS. Elemental analyses were measured by conventional element analyzer. UV−vis spectra were recorded in a conventional quartz cell (light path 10 mm) on a UV spectrophotometer equipped with a temperature controller to keep the temperature at 25 °C. Fluorescence spectra, quantum yields, and fluorescence lifetimes were measured with an FLS spectrometer by employing the time-correlated single-photon-counting (TCSPC) technique. For fluorescence lifetimes, the instruments equipped with a nanosecond flash lamp, typically 5000 counts, were collected at the peak channel, and the decay curves were fitted by least-squares deconvolution with original Instrument software; the quality of the parameters was judged by the reduced χ^2 values and the randomness of the weighted residuals. The absolute quantum yields were measured by using an integrating sphere with an inner diameter of 150 mm, coated inside with $BaSO_4$, and calculated by using following equation:

$$\Phi = \frac{f}{\alpha} = \frac{\int L_{\text{emission}}}{\int E_{\text{solvent}} - \int E_{\text{sample}}}$$

where f is the photons emitted by the sample; Φ is the absolute quantum yield; L_{emission} is the luminescence emission spectrum of the sample, collected using the sphere; E_{sample} is the spectrum of the light used to excite the sample, collected using the sphere; and E_{solvent} is the spectrum of the light used for excitation with only the solvent in the sphere, collected using the sphere.

Atomic Force Microscopic (AFM) Measurements. A 1.0×10^{-7} M sample solution was dropped onto newly clipped mica and washed with 1.0 mL of distilled water and then air-dried. The samples were examined with an AFM in the tapping mode in air at room temperature.

Transmission Electron Microscopic (TEM) Measurements. A 1.0×10^{-5} M sample solution was dropped onto a copper grid. The grid was then air-dried. The samples were examined by high-resolution TEM measurement at an accelerating voltage of 200 keV.

Dynamic Light Scattering (DLS) Measurements. A sample solution was prepared by filtering solutions (about 3 mL) through a 0.45 μm filter into a clean scintillation vial at the concentrations of 1.0×10^{-5} M. The samples were examined on a laser light scattering spectrometer equipped with a digital correlator at 636 nm at a scattering angle of 90° at 25 °C.

Computational Methods. The initial geometry of PMCD was taken from the crystal structure.[24] The starting structures of **1**, **2**, **1·2**, and **1·2·**PMCD were assembled by using the molecular mechanics and molecular dynamics simulation methods. All simulations were performed by using a Dreiding force field.[25]

Preparation of 3. A mixture of 3,4-di(prop-2-ynyloxy)benzaldehyde (3.27 mmol, 700 mg), excess pyrrole (15 mL), and TFA (100 μL) was stirred for 1 h at room temperature. Excess pyrrole was evaporated under reduced pressure and the crude product was subjected to column chromatography on silica gel with chloroform−methanol (v/v = 100:1) as eluent. The resulting dipyromethane was reacted with 2,3-dichloro-5,6-dicyanobenzoquinone (DDQ; 1.82 g, 8.02 mmol) in toluene (100 mL) for 5 min. Et_3N (5 mL, 45 mmol) and $BF_3 \cdot Et_2O$ (15 mL, 68 mmol) were added to the solution, which was allowed to stand for 1 h. After the treatment of a 1 M aqueous NaOH solution (200 mL), the toluene layer was separated; the pH of the aqueous phase was adjusted by 1 M HCl to about 5−6 and extracted by chloroform (3 × 50 mL). The combined organic phase was evaporated under reduced pressure, and the resulting crude product was purified by the column chromatography on silica gel with chloroform−petrol ether (v/v = 3:1) as eluent to obtain the desired compound **3** (13%). ^{1}H NMR (300 MHz, $CDCl_3$, ppm) δ 7.93 (s, 2H), 7.34 (m, 2H), 7.2 (m, 1H), 7.06 (d, 2H), 6.55 (d, 2H), 4.85 (m, 4H), 2.58 (m, 2H); ^{13}C NMR (300 MHz, $CDCl_3$

(24) Betzel, C.; Saenger, W.; Hingerty, B. E.; Brown, G. M. *J. Am. Chem. Soc.* **1984**, *106*, 7545–7557.

(25) Mayo, S. L.; Olafson, B. D.; Goddard, W. A., III *J. Phys. Chem.* **1990**, *94*, 8897–8909.

ppm) δ 150.0, 147.0, 143.8, 134.8, 131.5, 127.4, 125.0, 118.4, 117.1, 113.7, 56.8; ESI-HRMS calcd for $C_{21}H_{15}BF_2N_2O_2Na^+$ 399.1089, found 399.1085.

Preparation of 1. 6-Deoxy-6-azide-permethyl-β-cyclodextrin was prepared according to the literature procedures.[26] 6-Deoxy-6-azide-permethyl-β-cyclodextrin (0.4 mmol, 576 mg) and **3** (0.1 mmol, 37.6 mg) were dissolved in 15 mL of DMF, to which CuI (0.2 mmol, 38 mg) was added at once under nitrogen atmosphere. The solution was stirred at 70 °C for ca. 5 h, and additional CuI (0.2 mmol, 38 mg) was added to this mixture, keeping this temperature for 24 h. After cooling to room temperature, the mixture was filtered in order to remove any insoluble copper salt, and the filtrate was evaporated under reduced pressure to remove excess DMF. The residue was purified by silica gel column by using chloroform−methanol (v/v = 45:1) to obtain compound **1** (54%) as an orange−red solid. ^{1}HNMR (300 MHz, $CDCl_3$ ppm) δ 7.91 (s, 2H), 7.81 (s, 1H), 7.77 (s, 1H), 7.30 (m, 2H), 7.18 (m, 1H), 6.92 (d, 2H), 6.55 (d, 2H), 5.35 (m, 4H), 5.27 (s, 2H), 5.10−5.20 (d, 12H), 4.80−5.00 (m, 4H), 3.00−4.00 (m, 200H); ^{13}C NMR (300 MHz, $CDCl_3$ ppm) δ 151.0, 147.8, 146.8, 143.7, 142.8, 142.7, 134.7, 131.4, 127.1, 125.9, 125.7, 125.1, 118.4, 117.4, 114.0, 99.2, 98.9, 98.7, 98.3, 82.0, 81.8, 80.4, 80.4, 80.3, 79.8, 78.8, 71.5, 71.3, 71.0, 70.7, 70.6, 61.8, 61.6, 61.5, 61.4, 61.4, 59.2, 59.0, 59.0, 58.7, 58.5, 58.4, 51.2; MALDI-HRMS calcd for $C_{145}H_{233}BF_2N_8O_{70}Na^+$ 3279.4917 found 3279.4911. Anal. Calcd for $C_{145}H_{233}BF_2N_8O_{70}$: C, 53.47; H, 7.21; N, 3.44. Found: C, 53.52, H, 7.15, N, 3.43.

(26) (a) Hocquelet, C.; Blu, J.; Jankowski, C. K.; Arseneau, S.; Buisson, D.; Mauclaire, L. *Tetrahedron* **2006**, *62*, 11963–11971. (b) Reetz, M. T.; Waldvogel, S. R. *Angew. Chem., Int. Ed.* **1997**, *36*, 865–867.

Acknowledgment. We thank the 973 Program (2006-CB932900), NSFC (Nos. 20703025, 20721062, and 20932004), and the 111 Project (B06005) for financial support.

Supporting Information Available: NMR spectra, MS spectra, Job's plot, NOESY spectrum of **1**, TEM image, fluorescence control experiments, lifetime spectra, absolute quantum yield spectra, and negative ion mode ESI−MS. This material is available free of charge via the Internet at http://pubs.acs.org.